A Convective Wind Resource Model for Solar Vortex Power Generation

Amy M. Moore, Ph.D.[a]*, Michael O. Rodgers, Ph.D. [b], and Steven P. French, Ph.D. [b]

[a]*National Transportation Research Center, Oak Ridge National Laboratory, Knoxville, Tennessee, U.S.A.,* [b]*Georgia Institute of Technology, Atlanta, Georgia, U.S.A.*

mooream@ornl.gov*

Word count: 5,468

A Convective Wind Resource Model for Solar Vortex Power Generation

Climate change has increased the need for clean, non-polluting energy sources to decrease dependence on fossil fuels. Alternative energy sources, mainly solar and horizontal wind, have been the primary focus for producing clean energy. New technologies are being developed, such as the Solar Vortex (SoV), which was developed at the Georgia Institute of Technology, and relies on a vertical wind resource to generate power. The National Renewable Energy Lab (NREL) has resource models representing solar and horizontal wind resources across the 48 United States. This research developed a vertical wind resource model that is comparable in resolution to NREL's solar and horizontal wind resource models and uses the model for estimating power output for the SoV. This model complements NREL's existing resource models and supports deployment of an additional clean energy generation technology. The model was applied to Mesa, Arizona to find feasible sites for a small-scale vertical wind farm.

Keywords: convective wind resource; solar vortex; sustainable energy; geographic information systems; vertical axis wind turbine

1. Introduction

In an effort to reduce greenhouse gases (GHG), a number of renewable technologies have been developed to produce energy without burning fossil fuels. Hydropower has long been the main source of renewable energy. More recently wind and solar technologies have been deployed to generate electricity. In March 2015 they accounted for less than 10 percent of U.S. electricity generation (EIA, 2015). Most experts agree that significant progress towards clean energy will require the use of a wide variety of energy generation technologies.

This research focuses on one emerging technology: the Solar Vortex (SoV). The SoV generates energy using concentrated, convective wind. Using natural or artificial convective resources, the SoV has the ability to generate energy through the use of a turbine within the

unit. This research presents the development of a resource model that estimates where this technology can be used most effectively.

2. Review of Existing Models and Data Sources

2.1 Wind and solar resource models

2.1.1 Solar resource model

The National Renewable Energy Laboratory (NREL) has developed a U.S. solar resource model, representing data obtained from the State University of New York (SUNY) Albany's solar radiation model. The data displayed in the initial resource model was collected from 1985 to 2009, and contains average annual and monthly averages, measured in kilowatts per square meter, for the conterminous U.S. The resolution, depending on type, varies from approximately 10 to 40 square kilometers. Direct normal irradiance, global horizontal irradiance, and photovoltaic measurement types are provided (NREL, 2015).

For the purposes of this research, direct normal irradiance (in kilowatts per square meter) data were obtained for 2009. The data is in raster format, and was loaded into ArcGIS software, as shown in Figure 1: NREL's Solar Resource Model in ArcGIS (NREL, 2017). The resolution for this dataset is in 10 square kilometers. A Bird Clear Sky model was used to calculate the clear sky Direct Normal Irradiance (DNI). The sources for the data used in the model include radiance satellite imagery, snow coverage data, monthly average water vapor data, trace gases and aerosols data, and, where necessary, ground truth data. Due to variations in terrain and the existence of microclimates, the results of the model are accurate up to 15 percent of the measured values for each grid cell (NREL, 2012). As might be expected, this model shows that the western U.S. has the greatest potential for solar power generation.

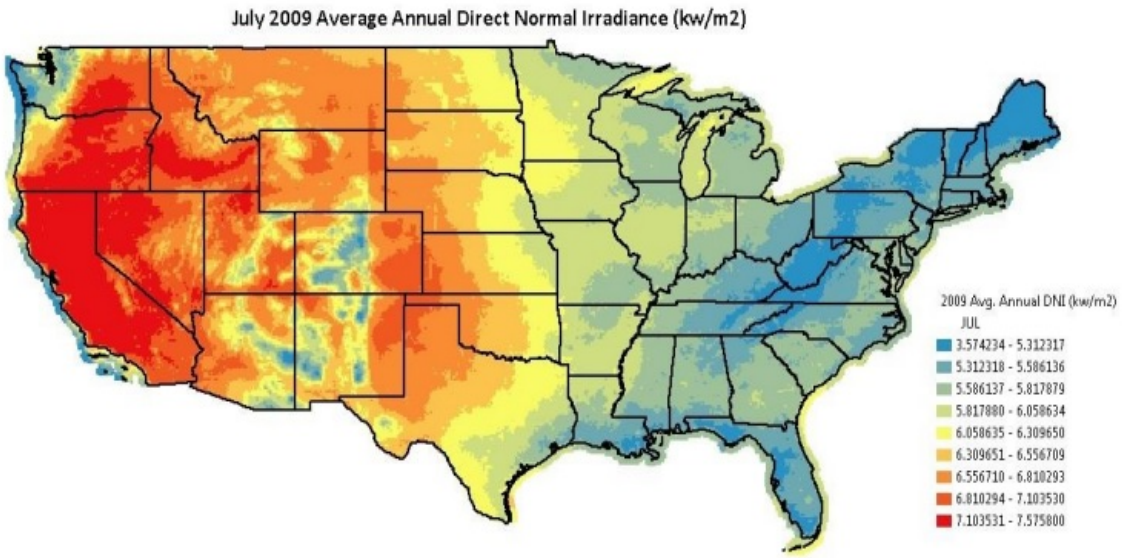

Figure 1: NREL's Solar Resource Model in ArcGIS (NREL, 2017)

2.1.2 Wind resource model

NREL's wind resource model displays estimated wind class values for the conterminous U.S. using data obtained from the Pacific Northwest National Laboratory's (PNNL) wind resource model, developed in October 1986. The data used in the model is at a resolution of 200 meters to one kilometer, with state-level measured data (excluding Alabama, Florida, Louisiana, and Mississippi) at 50-meter height hubs, and national-level data measured at 25-kilometer height hubs. The data were used in-conjunction with a model produced by a consulting firm, AWS TruePower, as an effort with the Department of Energy (DOE), to enhance the model and estimate wind class values for areas that were excluded in PNNL's model (NREL, 2015). This national resource model has been used in recent studies to evaluate the feasibility of different renewable energy technologies, and the methodology used to develop it has been used internationally for the same purpose (Anwarzai and Nagasaka, 2017).

The data accessed from the PNNL model excluded areas with low surface roughness, such as flat areas with low-lying vegetation, and areas with slopes greater than 20 percent. In areas with higher surface roughness, such as areas with forests and a thick vegetation canopy, the model assumes higher than actual wind potential. The model estimates wind class values based on varying surface roughness and slopes. In areas with adequate data, surface wind, coastal marine, and upper-air data measurements were obtained. In areas where the data were unavailable, wind speeds were estimated based on topographic features, amount of vegetation affected by wind, and in coastal regions, the existence of sand dunes and other wind-influenced features.

Wind class values one to seven were assigned, based on measured or estimated wind speed or wind speed potential, and these values were dependent upon the amount of data available in the model, topography, and wind variability (NREL, 2015). Areas with an assigned wind class of three to seven are considered suitable for large scale wind facilities, while areas with an assigned wind class of two are considered appropriate for small-scale and rural facilities. Areas with an assigned wind class of one are considered unsuitable for wind facilities (NREL, 2015).

For the purpose of this research, national-level data from August 2015 were obtained. The dataset was chosen because it did not contain any exceptions based on various topographic attributes. Because the data is at the national level, it is measured at a height of 25 meters, and the resolution is at one square kilometer. ArcGIS software was used to access the data, as shown in Figure 2: NREL's Wind Resource Model in ArcGIS (NREL, 2015). This model shows that many of the best sites for wind generation are offshore.

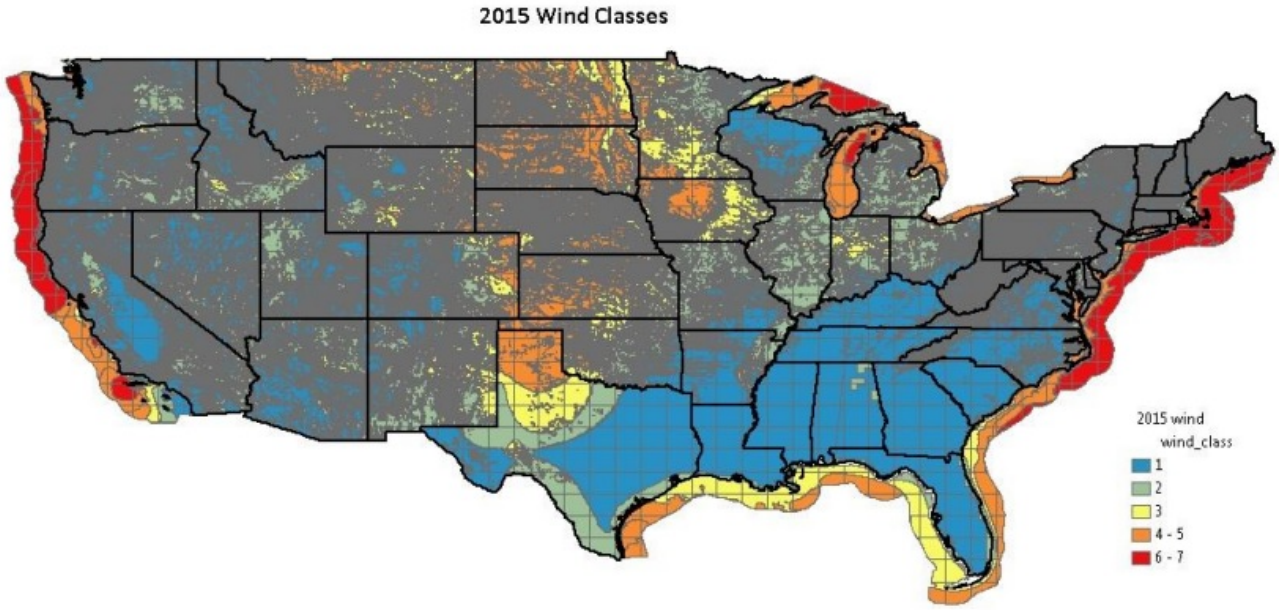

Figure 2: NREL's Wind Resource Model in ArcGIS (NREL, 2015)

2.1.3 Concentrated wind resource model

The current wind and solar resource models are sufficient for determining feasible locations for concentrated and distributed solar, and for utility-scale, horizontal wind turbines. However, there is currently no resource model for concentrated wind resource. A concentrated wind resource model is necessary for locating areas of the country that have convective potential, rather than advective potential, which is suitable for functional utility-scale wind turbines. Because convection is a small-scale resource, it is necessary that a concentrated wind resource model have a high resolution; one which is comparable to NREL's existing wind resource model (approximately one kilometer). Thus, an objective of this research was to create a resource model for a concentrated wind system. Such a resource model could be used to determine suitable locations for emerging technologies in concentrated wind.

2.1.4 SoV resource model

The SoV relies on the existence of a difference in temperature between the layer of warm air directly above the ground surface and the cooler air located directly above the warm air layer. This temperature differential theoretically exists in nature in varying locations. Theoretically, it can also occur in locations where the temperature differential is not naturally occurring, such as in man-made environments where there is a heat source located in a cooler environment. The SoV units rely on this temperature differential in order to create and sustain vortex formation within the unit. Therefore, it is necessary to locate areas where units could feasibly be constructed, such as in locations that are conducive to naturally occurring convection.

3. Methods

3.1 Concentrated wind resource model

3.1.1 The geographic information system (GIS) model

The geographic information system (GIS) resource model developed for this study was crucial in locating potential areas where concentrated wind energy production systems, such as the SoV, could potentially be installed based on existing natural resources. This GIS resource model was an important component for determining the viability of the SoV in varying locations based on potential power output. More importantly, it was necessary for resource evaluation to determine appropriate locations that may be suitable for future installation of concentrated wind energy production systems based on naturally occurring environmental attributes. The SoV relies on buoyancy. Many factors affect the SoV including: the density of air (based on the moisture content), ambient temperature, sensible heat flux (change in temperature from heat exchange) at the surface, latent heat (heat released or absorbed, causing a phase change, and is also related to moisture content), and physical

attributes (albedo and slope). The GIS resource model was used to calculate and pinpoint locations that contain the aforementioned resources necessary for potential funnel formation and sustainment within the SoV units due to convection. By developing a GIS resource model that determines resource availability with regards to temperature and heat exchange for the entire United States, many locations can potentially be considered for off-grid application of concentrated wind energy production facilities, like the SoV.

3.1.2 MODIS

The methods used by Ma et al (2010) were used in creating the GIS resource model, mainly the methods used to calculate sensible heat. Ma et al (2010) calculated sensible heat for the Tibetan Plateau using MODIS (Moderate Resolution Imaging Spectroradiometer) land surface temperature (LST) and emissivity satellite imagery data. MODIS, which is aboard the Terra satellite, which is part of the EOS (Earth Observing Satellites) system, views the entire earth in approximately two days. MODIS obtains data with 36 spectral bands. However, for the purposes of this study, only bands 31 and 32 were needed because those contain the surface and cloud coverage data and surface temperature data. The MODIS data were obtained from USGS. The files, which were an average temperature (in degrees Kelvin) of the first eight days of each month, were corrected for cloud coverage, and in raster format at one kilometer resolution, were downloaded directly from the database in hierarchical data format (HDF) and reprojected to geotiff format using the MODIS Reprojection Tool 4.1. There was a total of 13 MODIS raster files, covering the entire U.S., for four months (January, April, July, and October) for 2011 and 2013, at approximately 10:30 am and 10:30 pm (104 files total). An image of processed and reprojected MODIS files can be found in Figure 3: MODIS Land Surface Temperature and Emissivity, July 2013 (10:30 am).

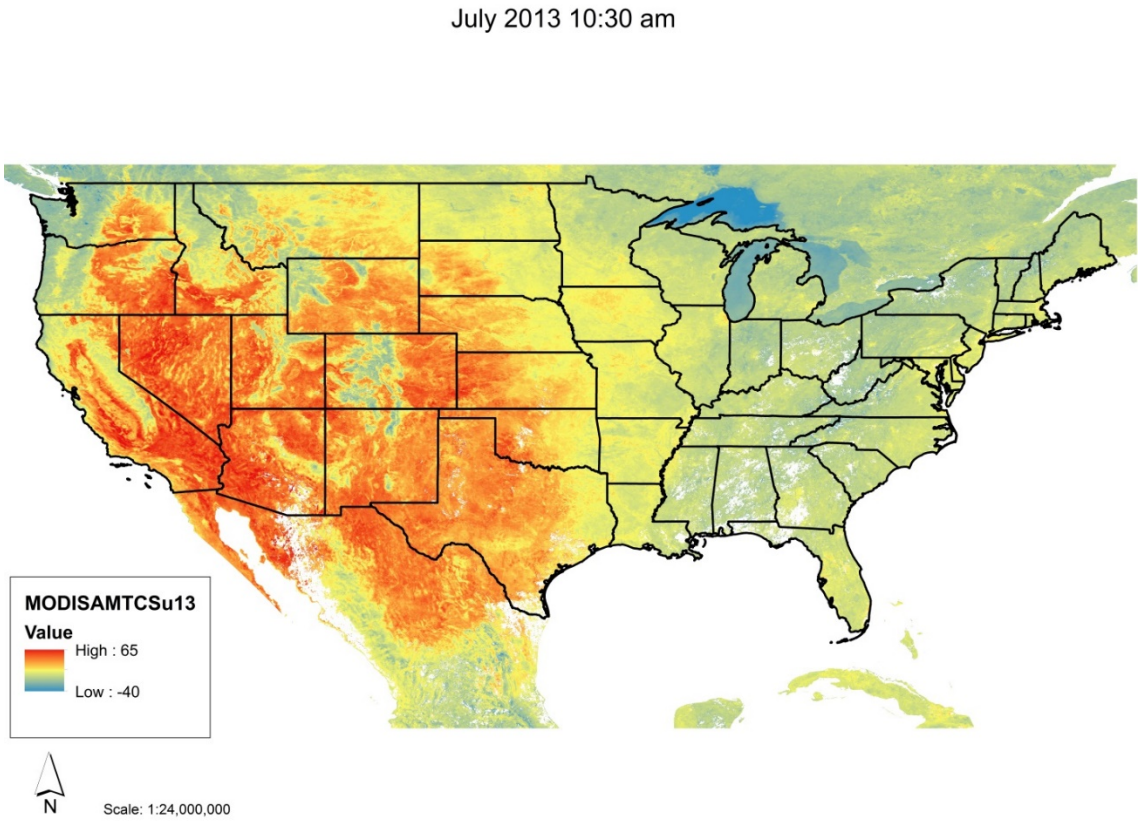

Figure 3: MODIS Land Surface Temperature and Emissivity, July 2013 (10:30 am).

3.1.3 Weather station variables

In order to calculate sensible heat for the conterminous U.S. using the methods outlined in Ma et al (2010), several weather variables were needed: air temperature (drybulb), wetbulb temperature, dewpoint temperature, relative humidity, and air pressure. Weather station data was needed from the National Oceanic and Atmospheric Administration (NOAA)'s National Environmental Satellite, Data, and Information Service (NESDIS), as part of the National Climatic Data Center (NCDC). For this study, published climatological data were accessed for each state from 12 different station locations for January, April, July, and October, for 2011 and 2013 at approximately 10:30 am and 10:30 pm. These data were used to create a point layer in ArcGIS to represent 216 collection stations across the U.S. The Kriging was used to perform an interpolation to obtain values across the U.S. After performing the

Kriging method of interpolation, 80 raster layers were created that would then be used to calculate sensible and latent heat.

3.1.4 Calculation of sensible and latent heat flux

For this study, as was the case in both Ma et al studies (2010 and 2013), it was necessary to calculate sensible and latent heat values over a heterogeneous landscape. The methods used in Ma et al (2010) were such that calculated sensible and latent heat values when using MODIS data along with surface layer data in areas with vast differences in landscape attributes were compared with sensible and latent heat values calculated from lower resolution MODIS and atmospheric boundary layer data in areas with similar landscape attributes to determine whether these methods resulted in values that were closer to those obtained from in-situ data measurements. The formulas used to calculate sensible and latent heat using surface layer data and MODIS data in this study were obtained from Ma et al (2010). For this study, it was determined that the calculations could be done solely using ArcGIS using the Raster Calculator tool. In order to perform the necessary calculations, several variables were needed.

3.1.4.1 Gamma calculation

The initial variable needed for the calculation was Gamma (Equation 1), or the Psychrometric constant, which was calculated using the following equation:

$$\boldsymbol{\gamma = 0.00066(1 + 0.00115T^{*})} \ \boldsymbol{(1)}$$

Where T* represents wet-bulb temperature in degrees Celsius, obtained from the weather station data.

3.1.4.2 Delta calculation

Delta (Equation 2), or the slope of the saturation vapor pressure deficit at air temperature, was calculated with the following formula:

$$\Delta = \frac{\boldsymbol{dp_{sat}}}{\boldsymbol{dT_a}} = \boldsymbol{d}(\mathbf{6.11} \times \mathbf{10}^{\left(\frac{\mathbf{7.5} \times \boldsymbol{T_a}}{\mathbf{273.3} + \boldsymbol{T_a}}\right)}) \Big/ \boldsymbol{dT_a} = \mathbf{25032.575295} \times \mathbf{10}^{\frac{\mathbf{7.5}\boldsymbol{T_a}}{\mathbf{273.3} + \boldsymbol{T_a}}} \times \frac{\mathbf{1}}{(\mathbf{273.3} + \boldsymbol{T_a})^{\mathbf{2}}} \mathbf{(2)}$$

Where $\boldsymbol{T_a}$ represents the air temperature at the reference height in degrees Celsius, which was obtained from the weather station data.

3.1.4.3 p^*_{sat} and VPD calculation

The following two formulas were obtained from *Principles of Environmental Physics*, (J. L. Monteith & M. H. Unsworth. Edward Arnold, Sevenoaks. 2nd edition, 1990):

p^*_{sat} (Equation 3), or the saturation pressure of water vapor at wet-bulb temperature was calculated using the following formula:

$$p^*_{sat} = 6.11 \times 10^{\left(\frac{7.5 \times T_a}{273.3 + T_a}\right)} (3)$$

Where T_a, is air temperature, which was obtained from weather station data, and measured in degrees Celsius. The result was calculated in millibars and converted to kilopascals.

VPD (Equation 4), or vapor pressure deficit, was calculated using the following formula:

$$\text{VPD} = (1 - (\varphi/100))^* p^*_{sat}) \ (4)$$

Where φ, or relative humidity, is obtained from weather station data, and p^*_{sat} was calculated in the previous equation. The result is measured in millibars and converted to kilopascals.

3.1.4.4 p_v *c*alculation

$\boldsymbol{p_v}$ (Equation 5), or the partial pressure of water vapor, was calculated using the following formula:

$$\boldsymbol{p_v} = \mathbf{6.11} \times \mathbf{10}^{\left(\frac{7.5 \times T_d}{273.3 + T_d}\right)} (5)$$

Where T_d represents the dewpoint temperature in degrees Celsius, which was obtained from weather station data, and the result was measured in millibars.

3.1.4.5 p_d calculation

$\boldsymbol{p_d}$ (**Equation 6**), or the partial pressure of dry air, was calculated using the following formula:

$$p_d = p - p_v \ (6)$$

Where p is actual pressure recorded at a measuring station, which was obtained from the station pressure interpolation layer, and $\boldsymbol{p_v}$was calculated previously.

3.1.4.6 ρ calculation

ρ (Equation 7), or air density, was calculated using the following formula:

$$\boldsymbol{\rho = \frac{p_d M_d + p_v M_v}{R T_a}} \ (7)$$

$\boldsymbol{M_d}$ = 28.964 gm/mol

$\boldsymbol{M_v}$ = 18.016 gm/mol

$\boldsymbol{R}$ = 8.31447 J/mol*k

Where $\boldsymbol{p_d}$ and $\boldsymbol{p_v}$ were calculated previously; $\boldsymbol{T_a}$ is air temperature in degrees Celsius, obtained from weather station data; the constant, $\boldsymbol{M_d}$, is the molar mass of dry air, measured in grams per mole; the second constant, $\boldsymbol{M_v}$, is the molar mass of vapor, measured in grams per mole; and the third constant, $\boldsymbol{R}$, is the universal gas constant, which is measured in Joules per mole kilogram.

3.1.5 Sensible heat calculation

Using the previous formulas, along with two additional variables, sensible heat (Equation 8) was calculated using the following formula:

$$H = \rho c_p \frac{T_0 - T_a}{r_{ah}} \quad (8)$$

c_p = 1005 Joules per kilogram Kelvin

r_{ah} = 80 for a.m. / 200 for p.m.

Where ρ, or air density, was calculated previously; the constant c_p is the air specific heat at constant pressure; T_0 is surface temperature, in degrees Celsius, obtained from MODIS; T_a is air temperature, obtained from weather station data; and the constant r_{ah} is the aerodynamic resistance for heat transfer between land and surface at the reference height, which varies depending on the time considered for the calculation (morning or night). The result is measured in watts per meter square. r_{ah} was determined by analysis of Ameriflux sites for differing land cover type classes, and represents how easily heat can leave a surface, with lower resistance resulting in heat leaving a surface faster. It is a function of atmospheric stability, wind speed, and surface roughness. It decreases with an increase in wind speed and an increase in surface roughness, and conversely, it increases with an increase in stability (Powell, 2003). Sensible heat estimates from the model can be found in Figure 4: Sensible Heat Flux, July 2013 (10:30 am).

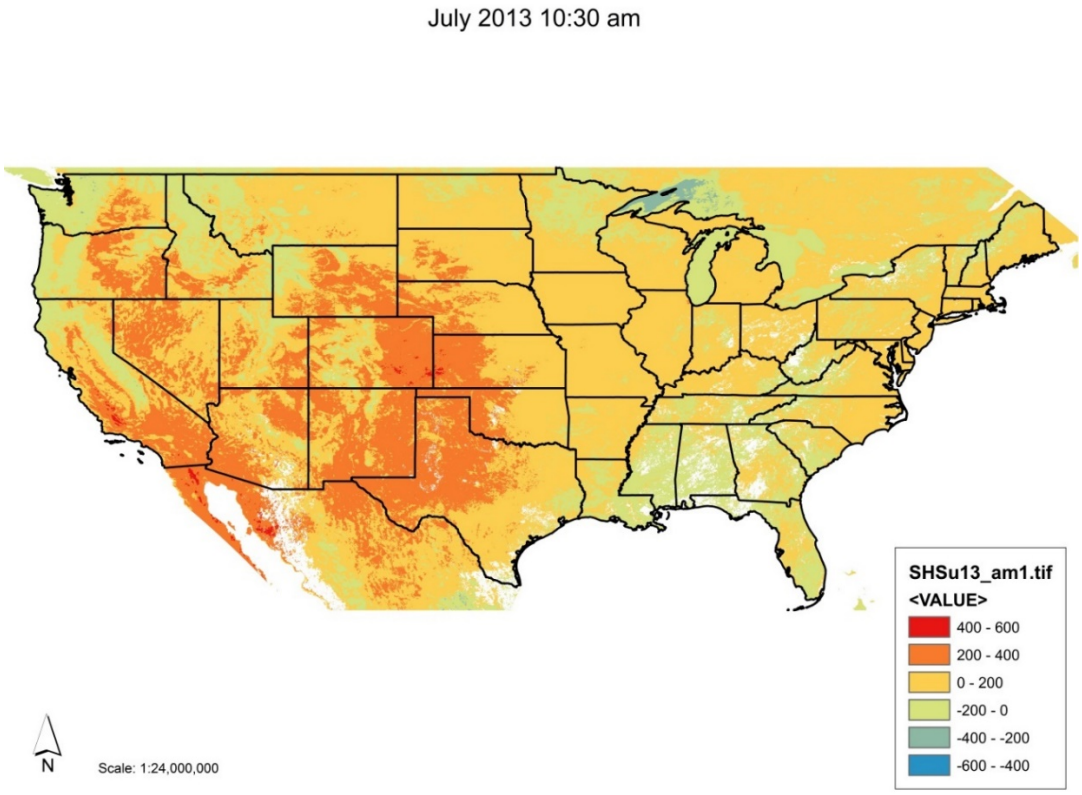

Figure 4: Sensible Heat Flux, July 2013 (10:30 am)

3.1.6 Latent heat calculation

The methods for calculating latent heat were obtained from Bonan (2002). Using the results obtained from the previous calculations and the interpolation layers, latent heat (Equation 9) was calculated using the following formula:

$$\boldsymbol{\lambda E} = \left(\frac{-\boldsymbol{\rho C_p}}{\boldsymbol{\gamma}}\right)\left(\frac{\boldsymbol{VPD}}{\boldsymbol{r_{ah}}}\right) \quad (9)$$

Where $\boldsymbol{\rho}$, $\boldsymbol{C_p}$, $\boldsymbol{VPD}$, $\boldsymbol{r_{ah}}$, and $\boldsymbol{\gamma}$ were all calculated previously. The results are measured in watts per meter square.

The raster calculator tool in ArcToolbox was used to perform the latent heat calculations based on the ASCE Standardized Reference Evapotranspiration Equations (Allen, 2005) for

saturated vapor pressure, actual vapor pressure, and the vapor pressure deficit, and using the weather station variable interpolation layers:

3.1.6.1 Saturation vapor pressure (Equation 10)

$$\boldsymbol{e_s = 0.6108 \times e^{\left(\frac{17.27 \times T_a}{237.3 + T_a}\right)}} \ (\mathbf{10})$$

$\boldsymbol{T_a}$ represents air temperature, which was obtained from the interpolation layer.

Actual vapor pressure (Equation 11)

$$\boldsymbol{e_a = \left(\frac{\varphi}{100}\right) \times e_s} \ (11)$$

Where $\boldsymbol{\varphi}$ represents relative humidity, which was obtained from the interpolation layer, and $\boldsymbol{e_s}$ represents saturation vapor pressure, which was calculated in the previous equation.

Saturation and actual vapor pressure deficit (Equation 12)

$$\mathbf{PD} = \boldsymbol{e_a - e_s} \ (12)$$

Where the pressure deficit is the difference between the actual vapor pressure and the saturation vapor pressure.

3.1.7 Contour elevation files to create digital elevation model (DEM)

A digital representation of variations in elevation was needed for the purpose of examining the landscape in areas that might be suitable for installation of SoV facilities. USGS's National Map Viewer contains data of various themes related to landscape attributes (i.e. contours, boundaries, orthoimagery, and transportation, among others). For the purpose of this study,

contour elevation files were obtained for each state, and these files were constructed using the 1/3 arc-second National Elevation Dataset (NED) from USGS at 30 square meters resolution. Using Python, 2,000 contour elevation files were loaded into ArcGIS to create a complete DEM, as shown in Figure 5: Completed Digital Elevation Model in ArcGIS.

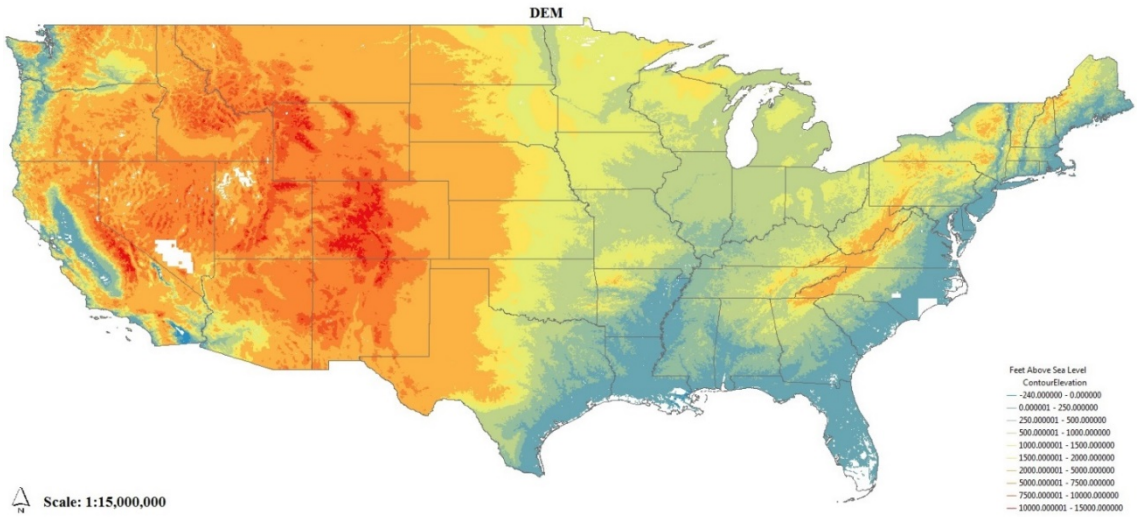

Figure 5: Completed Digital Elevation Model in ArcGIS

3.2 Slope model

A slope model was necessary for evaluating potential areas for installation of SoVs. Because a slope map for the entire U.S. was not readily available, one was created using the contour elevation files used in the creation of the Digital Elevation Model. Python was used to perform bilinear interpolation to estimate the values. Bilinear was chosen instead of the default nearest neighbor or cubic interpolation because bilinear is recommended for contour interval interpolation. The slope function calculated the degree of slope, rather than percent rise. Because the units of the State Plane projection were in U.S. feet, which were the same units used in the contour interval files, a z factor was not necessary to convert the units from

meters to feet. The completed model is shown in Figure 6: Completed Slope Model in ArcGIS.

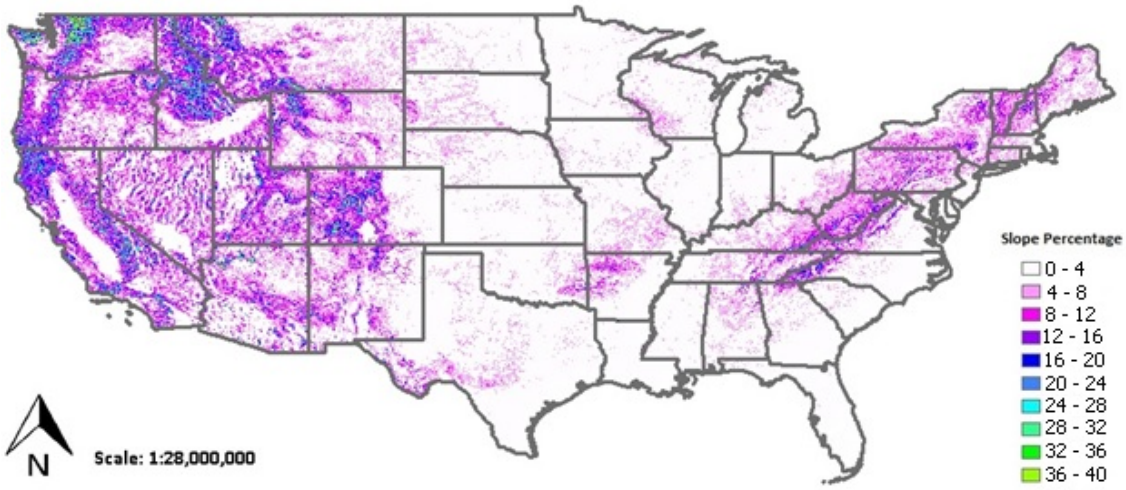

Figure 6: Completed Slope Model in ArcGIS

3.3 Threshold model

Estimated potential power output for the conterminous U.S. was performed using the sensible heat flux raster layers created in ArcGIS, in-conjunction with in-situ data of temporal distributions at varying physiographic regions across the U.S. The statistical computing and graphics software, R, was used to calculate power output based on the matrices in each sensible heat flux raster layer created in the GIS. Raster layers were created in R and imported back into the GIS. As with the resolution of the sensible heat flux raster layers, the results from the model are in one-kilometer resolution. Currently, the initial model used to estimate power output potential is lacking latent heat flux, and relies on sensible heat and temporal distributions of sensible heat across varying landscapes across the U.S. Later models will incorporate latent heat flux.

3.3.1 Represented distributions

In-situ data were necessary to validate the heat flux values calculated in the GIS, so locations were chosen to represent varying physiographic region types, and temporal distributions were obtained from these locations. The conterminous U.S. is divided into approximately 500 physiographic areas, which are divided into eight regions. 14 Ameriflux sites were chosen to represent these varying types of physiographic regions. Ameriflux, which is managed by the DOE and Lawrence Berkeley National Lab (LBNL), maintains monitoring sites across North and South America. Weather data, CO2, and heat flux, among other data, are measured at these different locations.

3.3.2 Analysis of in-situ data

The data obtained from Ameriflux consisted of heat flux, both sensible and latent, for the 14 sites, measured hourly, every day, for several years (typically from 2006 to 2012). Missing data was an issue; analysis of variance (ANOVA) tests were performed across the datasets for each site to determine statistical significance. For each site, the dataset with the least amount of data was chosen to represent the site. After the ANOVA was performed, data from previous years were used as substitutes for the missing data. Probability distributions were fit with a mixture of three normal distributions because many of the distributions had three peaks in the data. The mean μ, standard deviation σ, and percentage of the overall distribution which fell into each of the three distributions π were obtained, for each of the three normal distributions for each site (some sites, such as the Santa Rita Creosote site – where the former General Motors proving grounds and the SoV prototype are located, were bimodal, and only two normal distributions were needed). After these parameters were obtained, regression analyses were performed to determine how well the parameters for each of the distributions could be used to predict the overall means for the distributions at 10:30 am and 10:30 pm.

3.3.3 Threshold model steps

R was used to create a cell matrix in the AM sensible heat layer to perform the necessary calculations using the normal distributions created and regression coefficients for all 14 Ameriflux sites' sensible heat distributions. An arbitrary alpha value of 50 was used based on the assumption that the SoV would not be able to "start-up" until sensible heat measurements were at least 50 watts per meter square. Using the integrate function in R, the power output estimation was generated by simply integrating below the curve of the normally distributed sensible heat values associated with the Ameriflux sites. A beta value was applied using the completed power output raster layers in Raster Calculator. The beta value of 24.73 was obtained from results of the SoV prototype. This beta value represents the amount of sensible heat that the SoV unit will convert to vortex energy. The assumption is that, at 50 watts per meter square sensible heat, the relationship between sensible heat and vortex energy is linear. The completed model representing annual power output for 2013 is shown in Figure 7: 2013 Annual Power Output (from Threshold Model).

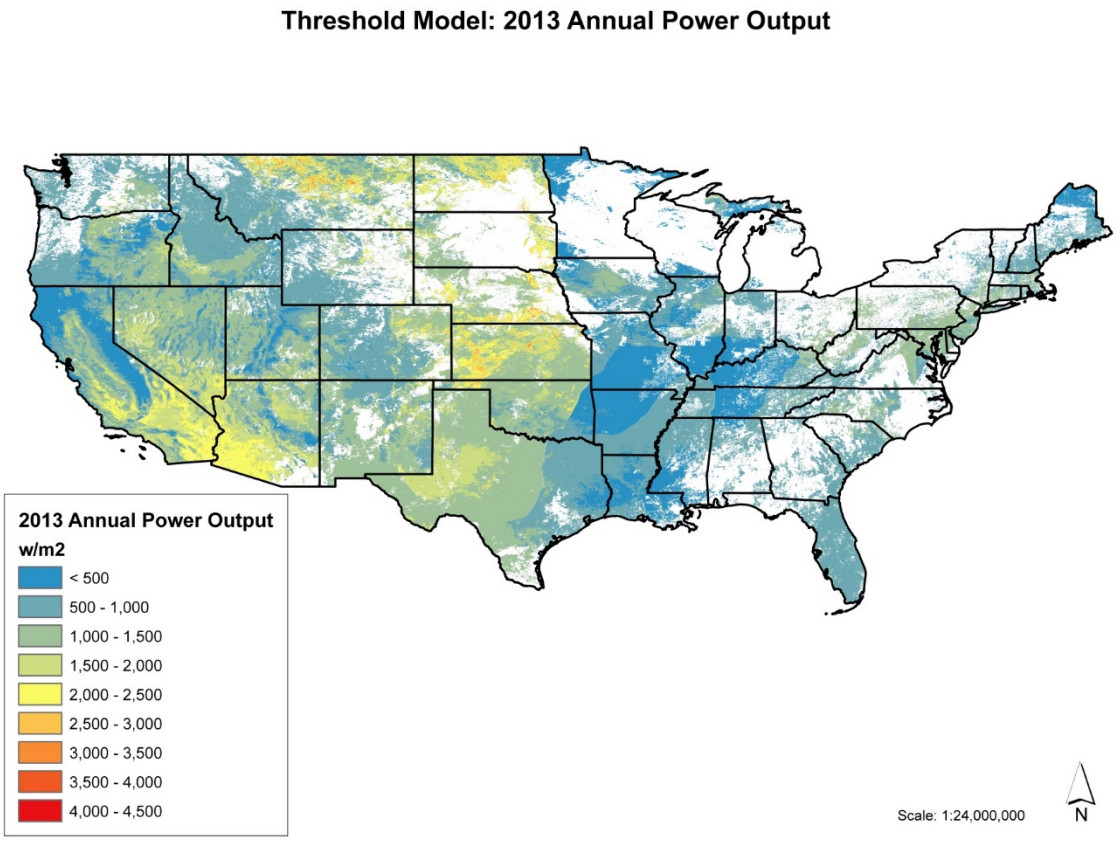

Figure 7: 2013 Annual Power Output (from Threshold Model)

3.4 Linear model assumptions

The final model incorporates the sensible and latent heat calculations, and the slope model to calculate potential energy generated by the SoV. For the purposes of this research, the completed model will be used to calculate vortex energy for Mesa, Arizona (location of SoV prototype).

3.4.1 Vortex power (Equation 13)

Based on Moore (2016) and on the results from the six-meter diameter SoV prototype located in Mesa, Arizona, it is assumed that:

$$Vortex\ Energy\ (VE) = (H)\ \text{x}\ (C_a)\ \text{x}\ (C_E)\ (13)$$

Where SoV power is a function of sensible heat H, the footprint of the SoV where sensible heat is obtained and utilized by the unit; the collection area, C_a, and measure of conversion efficiency C_E, by which the SoV converts sensible heat to power.

Using the six-meter diameter prototype located in Mesa, Arizona, it was found that, Vortex Energy for a unit with a diameter of six meters (Equation 14):

$$(VE)_6 = (1{,}500\ \text{kw}) = (237.4\ \text{w/m2}) \times (C_a) \times (C_E) =$$

$$(C_a)\ \text{x}\ (C_E) = \left(\frac{1500}{237.4}\right) = 6.32\ (14)$$

The collection area (C_a) represents the area around the SoV unit in which energy will be drawn into the unit. Both collection area (C_a) and the conversion efficiency factor (C_E) are unknown, but the assumption from this model is that the product of the two is equal to 6.32. Thus, for the final prototype model, which had a diameter of 10 meters, it is assumed that r^4, such that Vortex Energy for a unit with a diameter of 10 meters (Equation 15):

$$(VE)_{10} = 6.32 \times \left(\frac{10}{6}\right)^4 \times H = 6.32 \times 7.71 \times H$$

$$= 48.75 \times H\ (15)$$

Only sensible heat is considered in this model, due to the prototype being located in a desert, which lacks latent heat. Slope was also not considered for this model due to the flat location.

3.4.2 Daytime electrical power produced by SoV

Using the value obtained from the Vortex Power equation at a 10-meter diameter, it is then assumed that the daytime production power for the SoV (at approximately 10:30 AM) daytime electrical power (Equation 16) can be found using:

$$VE_D = (VE)_{10} \times (G_E) \quad (16)$$

Where the generation efficiency factor, G_E, is either .3, .4, or .5, representing a 30 to 50 percent efficiency in the unit converting sensible heat to electrical power.

3.4.3 Average daytime electrical power produced by SoV

The average daytime electrical power produced $(VE_{AD} - \text{Equation } 17)$ by the unit can then be determined by multiplying the daytime electrical power produced by a conversion factor (Equation 18) obtained from the Ameriflux data. The conversion factor (Equation 18) is based on the ratio of the measured sensible heat flux at the Ameriflux site located in the same physiographic region as the location used in the model, and the sensible heat flux obtained from the GIS results. For Mesa, Arizona, the Santa Rita Creosote site was used, resulting in:

$$(VE_{AD}) = (R_F) \times (VE)_{10} \times (G_E) \quad (17)$$

For the Santa Rita Creosote site, the conversion factor is:

$$(R_F) = \left(\frac{154}{148}\right) \quad (18)$$

3.4.4 Average monthly daytime electrical power produced by SoV

Lastly, to find average monthly daytime electrical power production, VE_{AM}, (Equation 19) the average daytime electrical power is used to calculate the following:

$$VE_{AM} = \left(\frac{VE_{AD} \times 12 \times 30}{1000}\right) \quad (19)$$

The result is measured in kilowatt-hours.

3.4.5 Average daytime electrical power produced by SoV for all locations

For all other locations where latent heat and slope are factors, the final model (Equation 20) is:

$$(\boldsymbol{VE}) = (\boldsymbol{R_F}) \times 48.75 \times (\boldsymbol{H} + .\boldsymbol{1\lambda E}) \times \left(1 + \left(2 \times \left(\left(\frac{\boldsymbol{\delta}}{\boldsymbol{100}}\right)\right)\right)\right) \times (\boldsymbol{G_E}) \quad (20)$$

Where sensible heat $\boldsymbol{H}$ and latent heat $\boldsymbol{\lambda E}$ and slope $\boldsymbol{\delta}$ were calculated in the GIS, and the result is measured in kilowatt-hours.

3.4.6 Relationship between sensible and latent heat and slope

It was assumed that both latent heat and slope extend operational time of the SoV. Latent heat, which is assumed to be approximately 10 percent as effective as sensible heat, was considered in the model, as the sum of sensible heat and 10 percent of the latent heat (Equation 21):

$$(H + .1\lambda E) \quad (21)$$

It was also assumed that two percent of each percent of slope (Equation 22) will extend the operational time of the SoV. As mentioned previously, it was assumed that, although an SoV

facility will need to be installed on level ground, upward or downward swept winds from sloping ground adjacent to the facility may influence the start-up time.

$$(1 + (2 \times ((\frac{\delta}{100}))) \quad (22)$$

3.4.7 Potential withdrawal of power

Final vortex energy is assumed to fall within a range of 30 to 50 percent of the energy calculated by the model. It is assumed that 30 to 50 percent of the energy will be converted to electricity by the SoV unit, with 30 being the lower estimate, 40 being an intermediate estimate, and 50 being the upper estimate.

4. Results

4.1 Mesa, Arizona calculation

In order to estimate Vortex Energy for Mesa, Arizona, the sensible and latent heat layers (AM values only), the power output estimation layer and table containing the average, monthly sensible heat values from Ameriflux, and the slope model were needed to perform the calculations. The completed July 2013 monthly average daytime vortex energy estimations can be found in Figure 8: Mesa, Arizona Summer 2013 Vortex Energy (Low Estimate), Figure 9: Mesa, Arizona Summer 2013 Vortex Energy (Medium Estimate), and Figure 10: Mesa, Arizona Summer 2013 Vortex Energy (High Estimate).

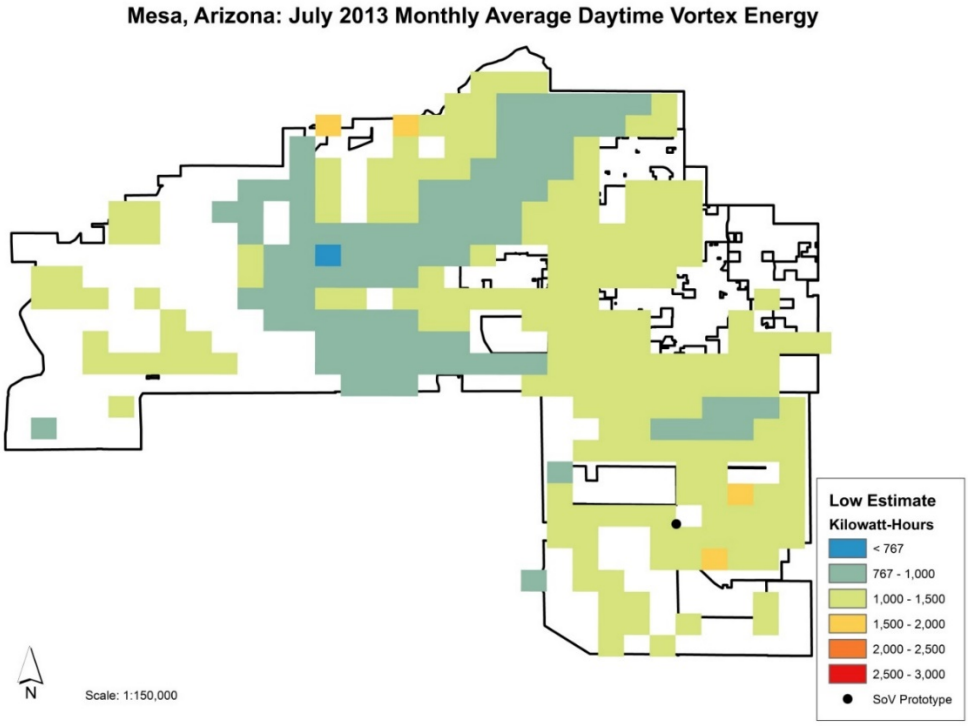

Figure 8: Mesa, Arizona Summer 2013 Vortex Energy (Low Estimate)

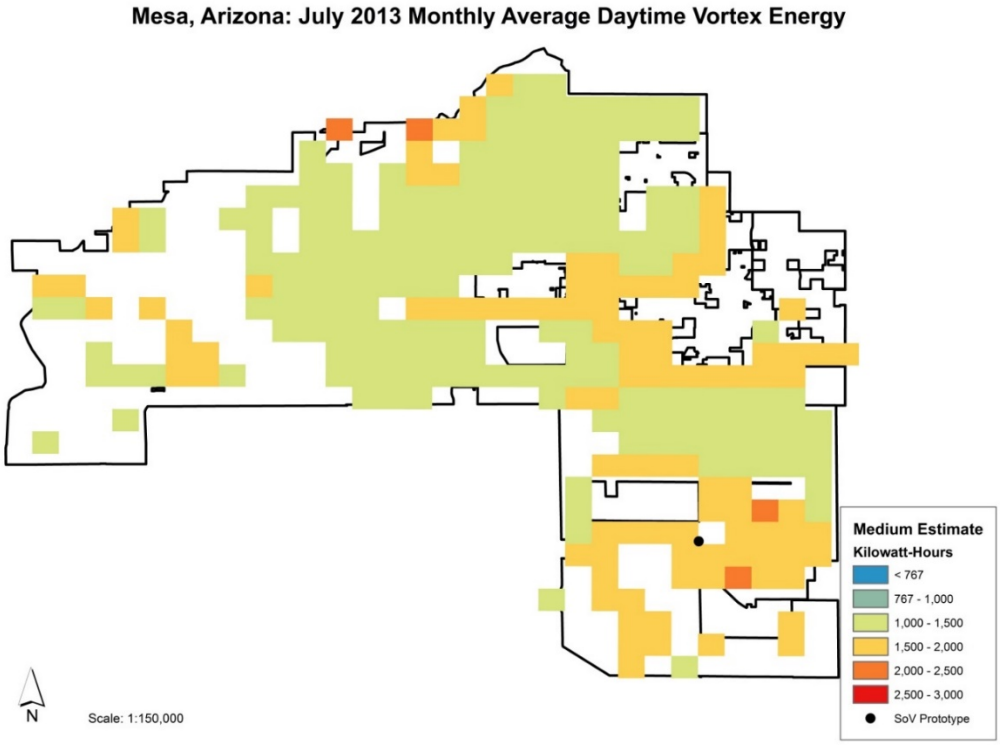

Figure 9: Mesa, Arizona Summer 2013 Vortex Energy (Medium Estimate)

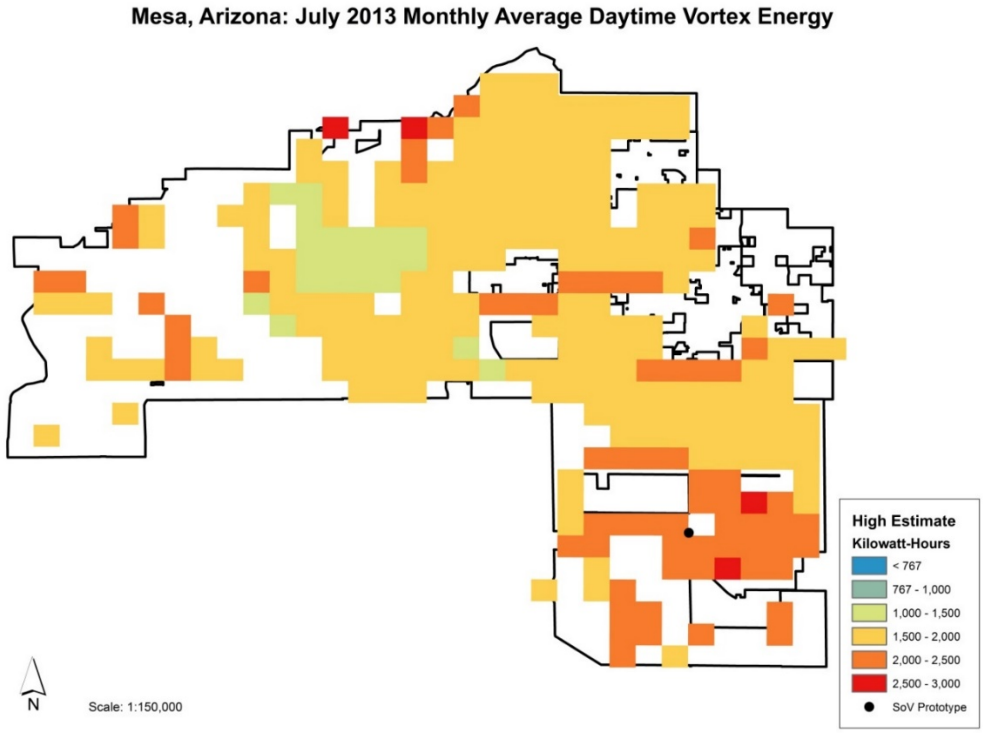

Figure 10: Mesa, Arizona Summer 2013 Vortex Energy (High Estimate)

5. Conclusions

The Solar Vortex (SoV) is a promising new technology. Initial tests suggest it is a viable alternative to other renewable energy technologies in certain locations. The resource model developed and presented here is useful in depicting locations where the SoV can be used. It shows that areas in Texas and the southwest that have intense solar radiation are the most promising locations for SoV technology. However, other factors such as slope, are also important in determining the effectiveness of this technology. This resource model should be considered a complement to the solar and horizontal wind resource models produced by NREL. As such, it will be useful to those considering renewable energy technology that requires convective, especially concentrated, vertical wind resource.

A goal of this research was to develop models that could be used to estimate SoV power production for the entire U.S. Although the models were only demonstrated in a small area in this research (Mesa, Arizona), the models can be applied to the entire 48 conterminous U.S.

Upon further testing of the SoV prototype, and further improvement of the linear and threshold models developed in this research, SoV power production can then be estimated for the entire U.S. This research shows that the Solar Vortex is an additional method for generating electric power. While this research shows this technology is not applicable everywhere, it identifies significant areas where this technology has significant potential.

6. Acknowledgements

1. The work performed for this manuscript was funded by the Department of Energy through the Advanced Research Projects Agency – Energy.

7. References

1) Allen, R. G. (2005). "The ASCE Standardized Reference Evapotranspiration Equation."
2) Anwarzai, M. and Nagasaka, K. (2017). "Utility-scale implementable potential of wind and solar energies for Afghanistan using GIS multi-criteria decision analysis." Renewable and Sustainable Energy Reviews, 71, pp. 150-160.
3) Bonan, G. (2002). Ecological Climatology: Concepts and Applications. New York: Cambridge University Press.
4) Bureau of Land Management. (2014). "Wind Energy Development Programmatic EIS." <http://www.windeis.anl.gov> (July 2015).
5) Environmental Protection Agency. (2015). "Overview of Greenhouse Gas Emissions."
6) Environmental Protection Agency. (2015). "Sources of Greenhouse Gas Emissions."
7) Georgia Institute of Technology. (2013). "Fluid Mechanics Research Laboratory."
8) Jahangiri, M., Haghani, A., Shamsabadi, A. A., Mostafaeipour, A., and Pomares, L. M. (2019). "Feasibility study on the provision of electricity and hydrogen for domestic purposes in the south of Iran using grid-connected renewable energy plants." Energy Strategy Reviews, 23, pp. 23-32.
9) Ma, Y., Menenti, M., & Feddes, R. (2010). "Parameterization of Heat Fluxes at Heterogeneous Surfaces by Integrating Satellite Measurements with Surface Layer and Atmospheric Boundary Layer Observations." Advances in Atmospheric Sciences, 27(2), 328-336.
10) Ma, Y., Han, C., Zhong, L., Wang, B., Zhu, Z., Wang, Y., and Amatya, P. (2013). "Using MODIS and AVHRR Data to Determine Regional Surface Heating Field and Heat Flux Distributions Over the Hetergeneous Landscape in the Tibetan Plateau." Theory of Applied Climatology, 117(3-4), 643-652.
11) Moore, Amy. (2016). Meeting off-grid transportation energy needs: A resource evaluation model for a solar vortex power generation system. Georgia Institute of Technology: SMARTech Repository.
12) Monteith, J.L. and Unsworth, M.H. (1990). Principles of Environmental Physics. Seven Oaks. 2nd Edition.

13) National Aeronautics and Space Administration. (2016). “Scientific Consensus: Earth’s Climate is Warming.”
14) National Renewable Energy Lab. (2015). “Dynamic Maps, GIS Data, and Analysis Tool.
15) National Renewable Energy Lab. (2015). “Dynamic Maps, GIS Data, and Analysis Tool.”
16) National Renewable Energy Lab. (1998). “Using CNG Trucks in National Parks.”
17) National Renewable Energy Lab. (2012). “Metadata on NREL Solar DNI Data.”
18) Powell, M., Vickery, P., and Reinhold, T. (2003). Reduced Drag Coefficient for High Wind Speeds in Tropical Cyclones. *Nature* 422, 279-283.
19) Simpson, M., Pearlstein, A., and Glezer, A. (2013). “Electric Power Generation Using Buoyancy-Induced Vortices.” Renewable Energy and Power Quality Journal, (11).
20) U.S. Energy Information Agency. (2015). “Electric Power Monthly.”